Available online at www.sciencedirect.com
SCIENCE DIRECT®
International Journal of Heat and Fluid Flow 24 (2003) 774–783
International Journal of HEAT AND FLUID FLOW
www.elsevier.com/locate/ijhff

Thermodynamic modeling and simulation of cavitating nozzle flow

C. Vortmann [a,*], G.H. Schnerr [b], S. Seelecke [c]

[a] Forschungszentrum Karlsruhe, Institut für Kern- und Energietechnik, Hermann-von-Helmholtz-Platz 1, 76344 Eggenstein-Leopoldshafen, Germany
[b] Lehrstuhl für Fluidmechanik, Fachgebiet Gasdynamik, Technische Universität München, 85747 Garching, Germany
[c] Department of Mechanical and Aerospace Engineering, North Carolina State University, 3211 Broughton Hall, Raleigh, NC 27695-7910, USA

Received 2 June 2001; accepted 15 January 2003

Abstract

Numerical simulations of cavitating flows are frequently performed by applying simple law of state-cavitation models. Here, the phase transition criterion is usually defined by assuming that cavitation occurs, if the pressure drops below the equilibrium vapor pressure. Since this simple modeling should be improved, an advanced method is developed, which takes phase non-equilibrium effects into account. The inclusion of non-equilibrium effects is important for future simulations of high-speed flows in very small-scale injector nozzles. Related to the van der Waals theory, the new approach is based on postulating Gibbs free energy for the phase mixture. This leads to a rate equation for quality. The two-phase flow is treated numerically by combining the rate equation with a volume-of-fluid algorithm. Unsteady calculations of cavitating flow in a converging–diverging passage and in a channel with a triangular obstacle show cyclically developing cavitation zones. The capability of this model to predict typical effects of cavitation, e.g. the formation of a re-entrant jet, is studied. Simulation of cavitating flow in the channel with a triangular obstacle is compared with the experiment and with numerical investigations of other authors.

Keywords: Cavitation; Two-phase flow; Equation-of-state; Van der Waals; Landau; CFD; Volume-of-fluid; Injection nozzles

1. Introduction

Since cavitation phenomena occur in a large number of hydraulic machines, e.g. pumps and ship's screws, there is an industrial interest in avoiding of damage or noise generation due to cavitation. In some applications it is desirable to make use of cavitation in order to increase the efficiency. For instance, quality of the atomisation process downstream of injector nozzles of diesel engines can be improved by evaporation of the fuel before injection. To achieve a better atomisation in such a way, cavitation control and further understanding of the cavitation process are necessary. This is obtained by numerical simulations, by means of which the flow structure is resolved in detail. Since the huge velocity and pressure gradients in the flow through injector nozzles yield numerical stability problems even under single-phase flow conditions, basic investigations concerning the cavitation model are carried out for simpler nozzle geometries in this study.

Within the scope of Computational Fluid Dynamics, two-phase flow is often treated as a homogeneous phase mixture. A homogeneous mixture consists of a single fluid of varying density ρ. Density variation is determined by a cavitation model. In technical literature, cavitation modeling is often based on either bubble growth models (Sauer, 2000) or 'equation-of-state' models. In the 'equation-of-state' method, presented first by Delannoy and Kueny (1990), density ρ is related to the pressure p at constant temperature T. In the ideal case, phase transition occurs in this model, if the pressure drops below the equilibrium vapor pressure. For reasons of numerical stability, the region, where phase transition takes place, usually covers a certain pressure interval. However, the physical modeling is rough and has to be improved. Phase transition is considered to be a molecular exchange process that develops during a finite time interval. Hence, the liquid will not immediately evaporate completely when the equilibrium vapor pressure is reached, but a time-depending evaporation

* Corresponding author.
E-mail address: claas.vortmann@iket.fzk.de (C. Vortmann).

0142-727X/$ - see front matter © 2003 Elsevier Inc. All rights reserved.
doi:10.1016/S0142-727X(03)00003-1

Nomenclature

A	austenite
$\vec{c}$	velocity vector
f	frequency
$\not{f}$	specific Helmholtz free energy
g	specific Gibbs free energy
h	height
K	probability
k	Boltzmann constant
m	mass
M_+, M_-	martensitic twins
N	number of molecules
P	load
p	pressure
p_{vap}	vapor pressure
s	specific entropy
t	time
$\mathscr{T}$	period
T	temperature
u	specific internal energy
U	velocity
V	volume
v	specific volume
v_b	specific volume occupied by molecules
x	vapor quality (mass-specific)
y	liquid quality (mass-specific)

Greeks

α	vapor fraction (volume-specific)
Φ	potential energy
Δ	difference
Δ	deformation
ρ	density
σ	cavitation number
τ	relaxation parameter

Indices

bar	barrier
c	cluster
H_2O	water molecule
l	liquid
liq	liquid
v	vapor
vap	vapor
∞	far field

process starts. Such a non-equilibrium effect can be modeled by an approach suggested by Landau and Ginzburg, which is applied by Badur and Banaszkiewicz (1998). In the present study, the promising model of Achenbach and Müller (1985) is modified with the purpose of applying it to fluid dynamics and especially to the description of cavitation phenomena.

2. Physical approach—the modified Müller–Achenbach model

2.1. Thermodynamic basics

To explain the model developed, a short overview of thermodynamic basics shall be given. If the Gibbs equation is written as

$$\frac{\mathrm{d}g}{\mathrm{d}t} \leqslant -s\frac{\mathrm{d}T}{\mathrm{d}t} + v\frac{\mathrm{d}p}{\mathrm{d}t}, \tag{1}$$

where s denotes the specific entropy, g is the specific Gibbs free energy $g = u - T \cdot s + p \cdot v$, and u is the specific internal energy, it is seen easily that the expression on the right hand side of Eq. (1) is zero, if a system at constant temperature T and pressure p is considered. In this case, the specific Gibbs free energy g tends towards a minimal value which is reached in equilibrium. Let the specific volume $v = V/m$ be a time-dependent variable. Then, it follows from $\mathrm{d}g/\mathrm{d}t = 0$ that $\partial g/\partial v = 0$ is also valid. In the g, v diagram, equilibrium is therefore obtained when the specific Gibbs free energy reaches a minimum. In Fig. 1 the specific Gibbs free energy g of a van der Waals gas is shown for different values of the pressure p (Müller and Seelecke, 1993). For high pressure the absolute minimum of g is found approximately at $v = 0.025$ m^3/kg. This value corresponds to a liquid state in the p, v diagram. At low pressure, g reaches the absolute minimum at a high specific volume, i.e. in vaporous states. Phase transition occurs when the 'vapor minimum' reaches the level of the 'liquid minimum'. At this stage, coexistence of both phases yields minimal g values. The corresponding pressure determines the equilibrium vapor pressure.

The dashed lines in Fig. 1 indicate the spinodal borders that separate the unstable area from the metastable regions. Metastable means that the fluid is stable concerning small disturbances. For big disturbances, the metastable single-phase state changes to a stable two-phase state.

2.2. The model medium

In the present investigation, the original concept for shape memory alloys of Achenbach and Müller (1985) is treated as well known, as the basics of this modeling are described in fundamentals of thermodynamics by Müller (1994). Only to clarify the analogy between the

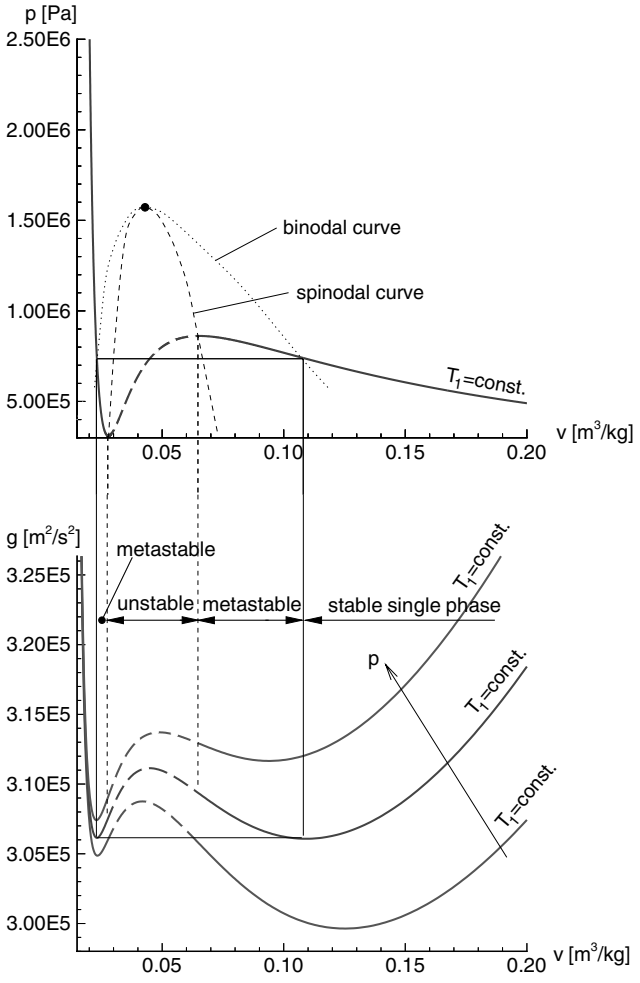

Fig. 1. Specific Gibbs free energy g of a van der Waals gas at constant temperature T_1 (Müller and Seelecke, 1993).

original concept for shape memory alloys and the modified model for water, the properties of shape memory alloys shall be reported briefly below. When subjected to a load P, these metallic alloys show plastic deformations due to phase changes of the metallic lattice. In Fig. 2, three different phase configurations are shown, the martensitic twins M_+ and M_- and the austenite A. The basic element of the model is a lattice particle. The martensitic twins may be considered versions of an austenitic particle, which are sheared by a load P. In shape memory alloys the phases are arranged in layers that contain several lattice particles. Each layer has a shear deformation Δ. Fig. 2 shows the postulated variation of the potential energy Φ under a shear load P of a layer. The potential energy Φ consists of an energetic potential depicted as a parabola corresponding to each phase. The equilibrium state of the metallic layer is characterised by the absolute minimum of the potential energy. In the present case, the absolute minimum is located in the M_+ area. The whole body is formed by many layers. The recent status of investigation concerning the description of shape memory alloys by the Müller–Achenbach model is presented by Seelecke and Müller (2003) and Seelecke (1999).

Analogy of the potential energy under a shear load for shape memory alloys and the specific Gibbs free energy of a van der Waals gas is obvious when comparing Fig. 2 (left) and Fig. 1. In both cases, an energetic potential is assigned to each phase. The energetic potentials change their positions depending on the load P and the pressure p, respectively. Therefore, it is reasonable to transfer the Müller–Achenbach concept to water.

At first, a model fluid comparable to the metallic lattice has to be designed. The water molecule serves as basic element. In contrast to the lattice particle, the water molecule is not deformed by a pressure change. But several water molecules may react to varying pressures by changing their occupied volume. For this reason, the concept of a cluster of molecules is introduced here. Each cluster consists of the same number of water molecules N_c and, thus, has the same constant mass

$$m_c = m_{H_2O} \cdot N_c, \tag{2}$$

where m_{H_2O} denotes the mass of a water molecule. The parameters m_c, m_{H_2O}, and N_c are specified in Section 2.4. A cluster does not form or change its mass. It is simply assumed that the material consists of small units of the same mass, in other words, of clusters. If a cluster grows, it therefore has to change its occupied volume V_c. This happens e.g. due to decreasing pressure. Changing the volume of a cluster V_c leads to a changing specific volume $v_c = V_c/m_c$, because the mass of a cluster m_c is constant. In analogy to the layer of lattice particles for shape memory alloys, an energetic potential is assigned to each phase for the specific Gibbs free energy of a cluster. Each cluster follows the same variation of the specific Gibbs free energy that is depicted in Fig. 2 (right). The clusters differ in their respective specific volume v_c. The clusters are situated at different places of the energetic potentials. If they manage to pass the energetic barrier at v_{bar}, they change their state of aggregation. Again, the complete model fluid consists of many clusters.

2.3. Rate equation for quality

The aim of this Section is to derive an expression for the change of quality with time, depending on the pressure and temperature variation. For this purpose, a rate equation for vapor quality $x = m_c/m$ is formulated similar to the original concept of Achenbach and Müller (1985)

$$\frac{dx}{dt} = \underbrace{(1-x)\cdot K_{l\to v}}_{\text{Gain}} \underbrace{-x \cdot K_{v\to l}}_{\text{Loss}}. \tag{3}$$

The gain of vapor clusters depends on the number of liquid clusters expressed by the liquid quality

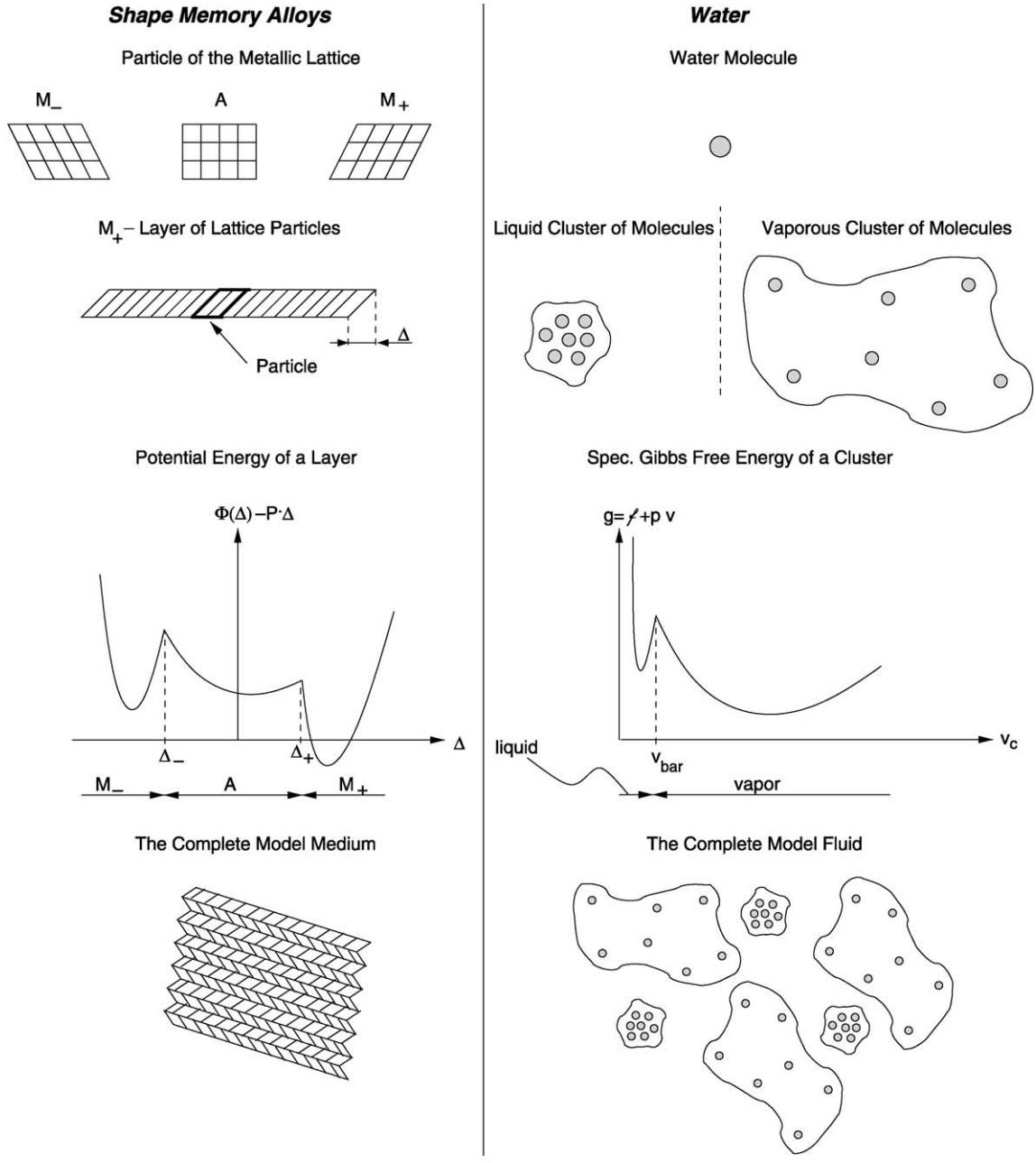

Fig. 2. Original model for shape memory alloys (Achenbach and Müller, 1985) and the modified Müller–Achenbach model for water.

$y = 1 - x = m_\mathrm{l}/m$, and further on the probability $K_{\mathrm{l}\to\mathrm{v}}$ of liquid clusters changing their state of aggregation from liquid to vapor. This probability can be derived by the theory of thermally stimulated processes (e.g. Chen and Kirsh, 1981), if the variation of the Gibbs free energy is postulated as described in Section 2.4

$$K_{\mathrm{l}\to\mathrm{v}} = \frac{\mathrm{e}^{-g(v_\mathrm{bar},p)/(k/m_\mathrm{c})T}}{\tau \int_{v=v_\mathrm{b}}^{v_\mathrm{bar}} \mathrm{e}^{-g(v,p)/(k/m_\mathrm{c})T}\,\mathrm{d}v}$$
$$K_{\mathrm{v}\to\mathrm{l}} = \frac{\mathrm{e}^{-g(v_\mathrm{bar},p)/(k/m_\mathrm{c})T}}{\tau \int_{v=v_\mathrm{bar}}^{v_\infty} \mathrm{e}^{-g(v,p)/(k/m_\mathrm{c})T}\,\mathrm{d}v}, \qquad (4)$$

where k is the Boltzmann constant. See Vortmann (2001) for a complete derivation of the probabilities. Here, it is sufficient to state that the numerator of $K_{\mathrm{l}\to\mathrm{v}}$ represents the number of clusters at the barrier (see Fig. 2 (right)), while the denominator is formed by the number of liquid clusters multiplied by the relaxation parameter τ. The probability $K_{\mathrm{v}\to\mathrm{l}}$ differs from $K_{\mathrm{l}\to\mathrm{v}}$ only in the integration boundaries that cover the region of the respective phase area. For example, the liquid area starts from the smallest possible specific volume v_b occupied by the molecules and ends at the barrier value v_bar.

Each g-potential drives phase transition in the direction of the respective phase. The ratio of the two

potentials consequently defines the time scale of the model. In addition, the quantitative value of the time scale is fixed by the relaxation parameter τ. Its value is determined in Section 4.2. The reciprocal value of the relaxation parameter describes a temperature-depending velocity of the phase transition. A more detailed discussion of its physical meaning can be found in Vortmann (2001).

2.4. Postulation of the Gibbs free energy

For Eq. (4), it is necessary to specify the specific Gibbs free energy g. Since cavitation is often referred to as 'cold boiling' (Isay, 1984), isothermal behavior at $T = 20$ °C is assumed. If g is specified for a single pressure, e.g. the vapor pressure p_{vap}, it is possible to calculate the specific Gibbs free energy at constant temperature for any pressure from

$$g = \not{f}(T, v) + p \cdot v. \tag{5}$$

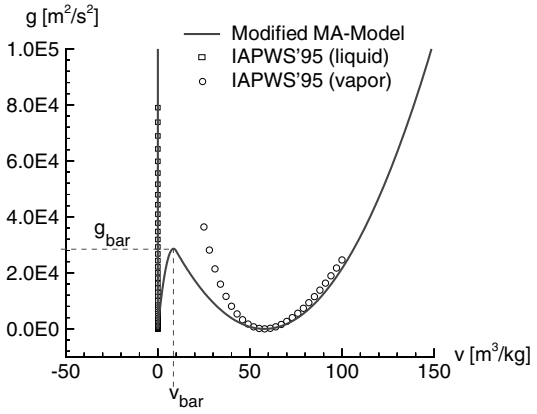

Fig. 3. Comparison of the specific Gibbs free energy postulated for the modified Müller–Achenbach model with values according to the IAPWS-95 equation of state (Pruß and Wagner, 2002), $p = p_v = 2340$ Pa, water at $T = 20$ °C.

Note that the specific Helmholtz free energy $\not{f}$ depends on T and v only, but not on the pressure p. The specific Gibbs free energy in the single-phase region can be determined from measurements. In the two-phase region, metastable and unstable states occur (see Fig. 1). In these regions, the specific Gibbs free energy cannot be measured. The measurements in the single-phase area are reproduced very well by the IAPWS-95 equation of state (Pruß and Wagner, 2002). The values of the specific Gibbs free energy according to IAPWS-95 are shown in Fig. 3. The minima represent transition from single phase to metastable states. Since the metastable g values depicted according to IAPWS-95 between the two minima are not verified, they can only give a direction. Using the modified Müller–Achenbach model the specific Gibbs free energy curve is approximated by three parabolas (see Vortmann, 2001). This allows to adjust the curvature in particular in the unstable two-phase region, where the Gibbs free energy is unknown, as stated above. Curvature in the two-phase region is represented mainly by the barrier height g_{bar} indicated in Fig. 3.

In order to specify the barrier height g_{bar} and the mass of a cluster m_c (necessary for Eq. (4)), additional information is needed. According to Section 2.1, phase transition at constant temperature takes place in the equilibrium at constant pressure, or to be more exact at the vapor pressure p_{vap}. It is therefore aimed at specifying g_{bar} and m_c in such a way that the model response yields an equilibrium phase transition at the constant vapor pressure (see Fig. 4). The model response shall be discussed in detail in Section 2.5. Here, it shall only be pointed out that this strategy leads iteratively to the barrier height shown in Fig. 3, and the mass of a cluster results in $m_c = 1.7 \times 10^{-24}$ kg. The iteration procedure consists in adjusting g_{bar} and m_c little by little, with the intention to constrain a model response at constant vapor pressure. Having the mass of a water molecule

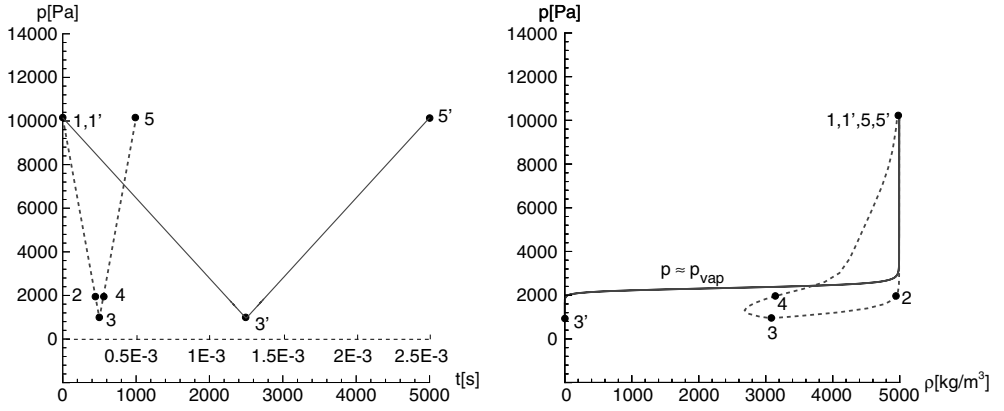

Fig. 4. Response of the model to slow and fast variation of the pressure, left: input, right: response, $\tau = 1 \times 10^{-4}$ s kg/m^3, $m_c = 1.7 \times 10^{-24}$ kg, water at $T = 20$ °C.

$m_{H_2O} = 30 \times 10^{-27}$ kg, it follows from Eq. (2) that a cluster consists of $N_c = 57$ water molecules.

2.5. Determination of the thermodynamic state

Having specified g and m_c, it is possible to solve the rate equation (Eq. (3)) in combination with Eq. (4). Quality in Eq. (3) is calculated by a routine that is particularly suited for stiff systems (Radau IIa from the book of Hairer and Wanner (1991)). The integrals in Eq. (4) are solved by using the commercial software NAG (2001). Fig. 4 shows a result of the modified Müller–Achenbach model. Response of the model to slow and fast pressure variation, respectively, is depicted in a p, ρ diagram. The density $\rho = 1/v$ is calculated from the quality using the well-known relation

$$1/\rho = x \cdot 1/\rho_v + (1 - x) \cdot 1/\rho_l. \tag{6}$$

For a slow pressure variation from point $1'$ ($\rho = \rho_l$) to $3'$ ($\rho = \rho_v$) and back to $5'$, model response to pressure increase and pressure decrease follows the same solid curve. Phase transition occurs approximately at the vapor pressure of $p_{vap} = 2340$ Pa along the horizontal line. Hence, for a slow pressure variation the expected equilibrium process is obtained with the values of $g_{bar} \approx 3 \times 10^4$ m^2/s^2 and $m_c = 1.7 \times 10^{-24}$ kg, as previously discussed in Section 2.4.

The time scale of the model and, thus, the border between equilibrium and non-equilibrium is controlled by the relaxation parameter τ that is set to $\tau = 1 \times 10^{-4}$ s kg/m^3. This assumption for the τ value is based on the experience gained from the original Müller–Achenbach model for shape memory alloys. A detailed discussion of the τ value is given in Sections 4.1 and 4.2. The rapid pressure change depicted in Fig. 4 by a dotted line from points 1–3 and back to 5 with a typical time scale of $t_{typ} = 0.5 \times 10^{-3}$ s yields a non-equilibrium process. For instance, a superheated state exists at point 2. The medium does not have enough time to reach the equilibrium state. The typical time scale is of the same order as the time scale of the flow problem discussed at the end of Section 4.1.

3. Numerical modeling

The CFD code is based on the numerical concept presented in detail by Ferziger and Perić (1996). The integral forms of the 2-D Euler equations are solved numerically by an implicit finite-volume method on non-orthogonally structured, single-block grids with a collocated arrangement of variables. Momentum and continuity equations are coupled by the SIMPLE algorithm. The phase mixture is simulated as a fluid of varying density ρ, whereas the pure phases of liquid density ρ_l and vapor density ρ_v are considered to be incompressible

$$\rho = \alpha \cdot \rho_v + (1 - \alpha) \cdot \rho_l, \tag{7}$$

where α denotes the vapor fraction $\alpha = V_v/V$, with V_v being the volume occupied by the vapor. V is the cell volume. Evaporation and condensation are described by a volume source term on the right hand side of the continuity equation

$$\nabla \cdot \vec{c} = -\frac{1}{\rho}\frac{d\rho}{dt} = \rho \cdot \left(\frac{1}{\rho_l} - \frac{1}{\rho_v}\right) \cdot \frac{dx}{dt}. \tag{8}$$

Here, the continuity equation is written in a non-conservative form, and Eq. (6) is taken into account. The source term is calculated by using Eq. (3). To overcome problems due to the high density variation between vapor and liquid at the cell faces, a modified volume-of-fluid algorithm is used. In the volume-of-fluid method, an additional transport equation is solved for the vapor fraction α

$$\frac{\partial \alpha}{\partial t} + \nabla \cdot (\alpha \vec{c}) = \frac{d\alpha}{dt} + \alpha \nabla \cdot \vec{c} = \frac{\rho_l}{\rho_l - \rho_v} \nabla \cdot \vec{c}. \tag{9}$$

The last expression is derived using Eq. (7). To obtain the transport equation for α implemented in the CFD code, the $\nabla \cdot \vec{c}$ operator on the right hand side of Eq. (9) has to be eliminated using Eq. (8). A more detailed description of this modified volume-of-fluid technique can be found in Sauer (2000). A summary of the governing equations is given in Appendix A.

4. Results

4.1. Simulation of cavitating flow in a converging–diverging passage

The cavitation model discussed in the previous sections is now used to simulate unsteady cavitating flow in nozzles. While the future aim will be to calculate cavitating flow in injector nozzles, it is first recommended to keep the numerical test case, i.e. geometry and boundary conditions, simple and to investigate the properties and performance of the physical model. For this reason, a converging–diverging passage was designed. Its wall contour varies smoothly particularly in the smallest cross-section. Pressure peaks caused by sharp bends in the passage contour have therefore been avoided in this stage.

Geometry and boundary conditions are shown in Fig. 5. At the exit cross-section, a constant cavitation number $\sigma_{Exit} = (p_{Exit} - p_{vap})/\rho_l \cdot U_{Inlet}^2 = 5.45$ is imposed. The large diffusor part leads to a pressure increase and, hence, forces the cavitation to vanish within the computational domain. Since the physical model described in Section 2.4 and further discussed in 2.5 is used, the model fluid is water at $T = 20$ °C and the mass of a cluster is $m_c = 1.7 \times 10^{-24}$ kg. Consideration of

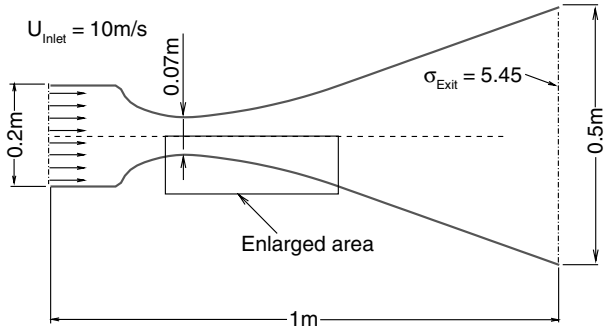

Fig. 5. Geometrical setup of a 2-D plane converging–diverging passage, inviscid calculation, $m_c = 1.7 \times 10^{-24}$ kg, water at $T = 20$ °C.

turbulence effects by an available $k\omega$ model was omitted, because it is intended to concentrate on flow phenomena caused by the cavitation model. Therefore, the mixture of water and steam is assumed to be inviscid.

While the variation of the Gibbs free energy and the mass of a cluster m_c were determined in Section 2.4 in order to approximate the equilibrium states, the time scale was chosen to be arbitrary to some extent. The time scale is fixed by the relaxation parameter τ. This parameter cannot be determined from the equilibrium, because an equilibrium state does not depend on time. Hence, the value of this parameter shall be specified from two-phase flow simulations below.

Fig. 6 presents the total vapor volume, integrated over the whole converging–diverging passage domain, versus time for different values of the relaxation parameter τ. Since the calculations for both parameter values τ start from a non-cavitating condition, periodic behavior is observed after passing a single overshoot. An influence of the relaxation parameter on the frequency cannot be found. The frequency of $f = 9.5$ Hz obviously is controlled by the geometry and boundary conditions. The curve of $\tau = 1 \times 10^{-4}$ s kg/m^3 does not only show a main maximum in each period, but a less intense second maximum. After the second maximum,

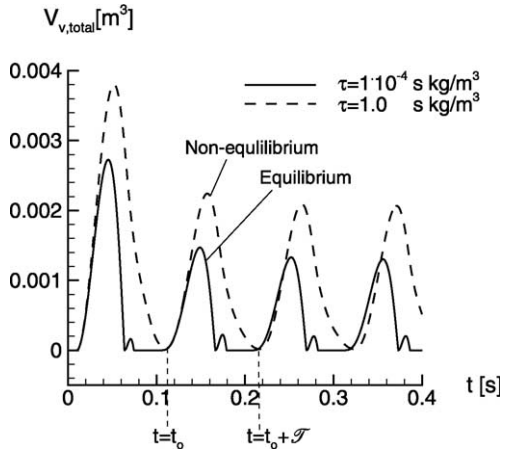

Fig. 6. Total vapor volume vs. time, variation of the relaxation parameter τ for the modified Müller–Achenbach model, $f = 9.5$ Hz.

the total vapor volume in the converging-diverging passage is zero. For $\tau = 1.0$ s kg/m^3, the vapor has vanished completely after the period of $t = t_o + \mathscr{T}$.

This behavior of developing and vanishing vapor volume is illustrated in Fig. 7. One cycle of the cavitating flow is shown in terms of velocity vectors and vapor fraction. For both parameters a cavitation zone grows behind the minimum cross-sectional area of the passage. At the cavity tail a sudden decrease of the vapor fraction occurs. This condensation induces suction to the surrounding water. This leads to the development of reverse flow, in other words, to the formation of a re-entrant jet. A re-entrant jet was often observed in experiments, e.g. by Stutz and Reboud (1997).

In contrast to $\tau = 1.0$ s kg/m^3, the value of $\tau = 1 \times 10^{-4}$ s kg/m^3 is characterised by a cavitation zone developing again at $t = t_o + \frac{9}{14}\mathscr{T}$ after cavitation had already vanished completely. When the re-entrant jet hits the main flow at $t = t_o + \frac{8}{14}\mathscr{T}$, a sudden pressure increase can be observed. The pressure increase causes the collapse of the cavitation cloud situated in the vortex. After the pressure wave has passed, the previous pressure level is reached again, and a new cavitation zone develops at $t = t_o + \frac{9}{14}\mathscr{T}$. This second cavitation cloud collapses while transported to the region of high pressure near the outlet. The second cavitation cloud causes the second maximum in Fig. 6 to appear, as was mentioned above.

In Fig. 8, the pressure distributions, together with the corresponding flow field, are depicted at $t = t_o + \frac{6}{14}\mathscr{T}$. At $\tau = 1 \times 10^{-4}$ s kg/m^3, cavitation zones match well with the area where the vapor pressure $p_{vap} = 2340$ Pa is reached, as is indicated by the black line. Hence, equilibrium states are obtained by this parameter value from thermodynamic point of view. At $\tau = 1.0$ s kg/m^3, the pressure is below the vapor pressure close to the minimum cross-sectional area of the passage only. There, vapor production takes place. The vapor is convected downstream, where it vanishes with delay due to the high value of the relaxation parameter τ. Since the pressure exceeds the vapor pressure in these downstream areas, subcooled non-equilibrium states exist. It is supposed that the model reacts with a delay to the rapid change of pressure: the higher the relaxation parameter τ is, the longer is the delay time.

This fact seems to be in contrast with the result shown in Fig. 4, where non-equilibrium states were obtained at $\tau = 1 \times 10^{-4}$ s kg/m^3 for fast pressure changes. Difference from the results discussed in the present Section is of course due to the coupling of the physical model with the flow field. If vapor is produced as a volume source (see Section 3), the pressure increases. Or to be more exact, the pressure is driven towards the equilibrium vapor pressure. Consequently, the parameter $\tau = 1 \times 10^{-4}$ s kg/m^3 yields states that are close to the equilibrium in the CFD simulation.

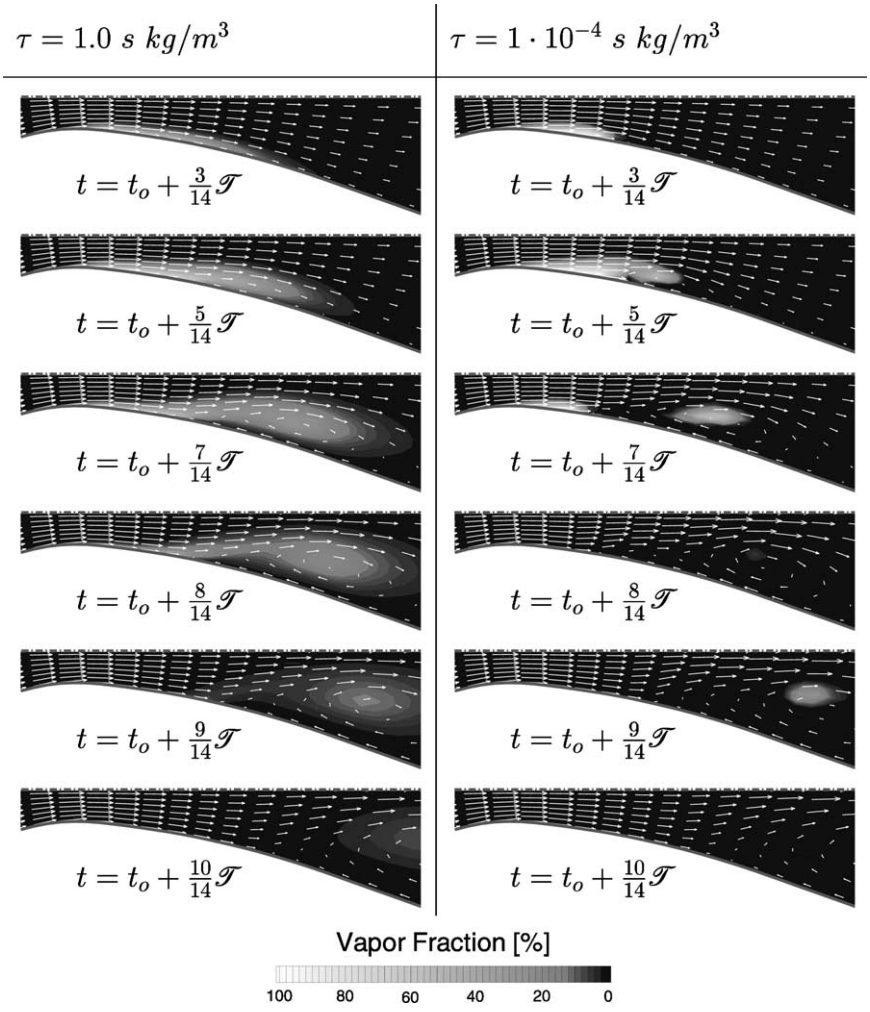

Fig. 7. Velocity vectors and vapor fraction for two different values of the relaxation parameter τ, $f = 9.5$ Hz.

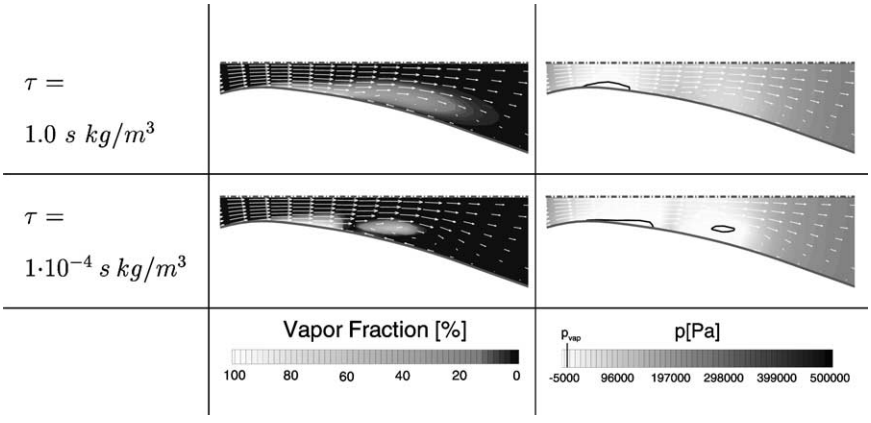

Fig. 8. Vapor fraction and pressure distribution for different values of the relaxation parameter τ, $t = t_o + \frac{6}{14}\mathcal{T}$, $f = 9.5$ Hz.

4.2. Simulation of cavitating flow in a channel with a triangular obstacle

Regarding the quantitative specification of the relaxation parameter τ in this section, simulation of cavitating flow is compared with experiments and with numerical investigations of other authors. The geometry investigated is shown in Fig. 9. It is taken from the experimental study of Lush and Peters (1982). Cavitating flow in this channel was studied numerically first by

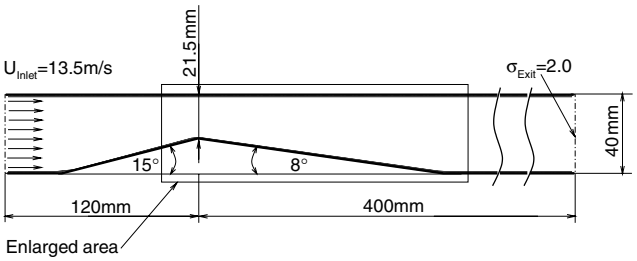

Fig. 9. Geometrical setup of a 2-D plane channel with a triangular obstacle, inviscid calculation, $m_c = 1.7 \times 10^{-24}$ kg, water at $T = 20$ °C.

Delannoy and Kueny (1990). According to the CFD investigation of Dieval et al. (1998), a constant cavitation number $\sigma_{\text{Exit}} = (p_{\text{Exit}} - p_{\text{vap}})/\rho_l \cdot U^2_{\text{Inlet}} = 2.0$ is imposed in the exit cross-section.

The velocity field and the vapor fraction distribution during the time interval $\mathscr{T} = 1/42$ Hz $= 0.024$ s are depicted in Fig. 10 relative to the main frequency. A result similar to those presented in Fig. 7 is obtained. This confirms the choice of the simpler geometry for basic investigations in Section 4.1. Fig. 10 shows that the cavitation zone starts growing from the minimum cross-sectional area of the channel. The formation of a re-entrant jet leads to the break-up of a cavitation cloud. The main frequency $f = 1/\mathscr{T} = 42$ Hz obviously represents the shedding frequency of the cavitation cloud.

In contrast to the results presented in Fig. 7, the cavitation zone at the minimum cross-sectional area of the channel depicted in Fig. 10 never vanishes completely. This is in qualitative agreement with observations made in the experiment of Lush and Peters (1982). It can be explained by the sharp bend in the channel contour, which causes a distinct pressure drop below the vapor pressure p_{vap}.

For smaller values of the relaxation parameter τ (see Vortmann, 2001), however, the attached cavitation vanishes completely for some time. When calculating higher τ values, a steady state appears. This is inconsistent with the break-up of the cavitation cloud observed in the experiment. The best result is obtained with the present value of $\tau = 1 \times 10^{-1}$ s kg/m^3. The calculation with $\tau = 1 \times 10^{-1}$ s kg/m^3 implies cavitation zones in areas of pressure levels far above the vapor pressure p_{vap} (see Section 4.1). This is not unusual, as stated e.g. by Dreiß (1997) for the cavitating flow in a centrifugal pump.

In agreement with the present simulations, numerical calculations of Dieval et al. (1998) show vortex shedding caused by cavitating flow. In contrast to the experiment, Dieval reports a process consisting of two vortexes during a single period, thus leading to two different cavitation clouds. The attached cavitation at the minimum cross-sectional area nearly vanishes for some time. Lush et al. measured an average shedding frequency of $f \approx 100$ Hz. In order to quantitatively match the experiments, further investigations have to be carried out. Three-dimensional and viscous/turbulent effects should be taken into account. Furthermore, surface tension should be added to the physical modeling of the phase change in order to introduce water quality effects due to nuclei sizes.

5. Conclusions

The first part of the present investigation deals with the development of a new cavitation model. The basic idea is to transfer a promising model, originally developed for phase changes of shape memory alloys, to phase changes of water. In this context, the Gibbs free energy of the phase mixture is postulated. The model defines the thermodynamic state, i.e. the relation of density ρ, pressure p, and temperature T, particularly in the two-phase region. It is shown that this model allows to adapt quantitatively the attributes of water at 20 °C during the phase transition. The method describes cavitation as a time-depending evaporation process.

In the second part, simulations of unsteady cavitating flows in nozzles are presented. Within the framework of the numerical method, a source term in the vapor fraction transport equation is calculated by the cavitation model discussed in the first part. Basic investigations are

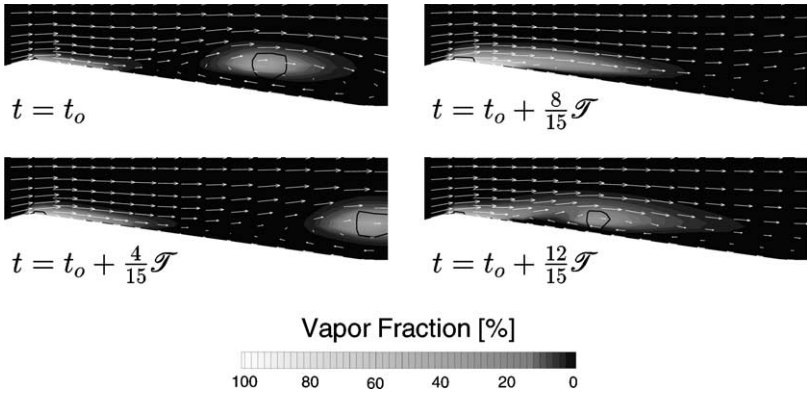

Fig. 10. Velocity vectors and vapor fraction, $\tau = 1 \times 10^{-1}$ s kg/m^3, $f = 42$ Hz.

carried out using a simple test case, a converging–diverging passage. It is demonstrated that the method is suited to resolve characteristic flow phenomena associated with cavitationm, e.g. the formation of a re-entrant jet. Equilibrium states or non-equilibrium states are obtained, respectively, depending on the choice of the relaxation parameter. The relaxation parameter determines the time scale of the model. Simulations of cavitating flow in a channel with a triangular obstacle show that the two-phase analysis employed is capable of reproducing flow structures comparable to those observed in the experiment, if a definite value is applied for the relaxation parameter. In order to quantitatively match the experiments, further numerical investigations will be performed.

Acknowledgements

Sincere thanks are given to Prof. Dr.-Ing. M. Perić from the TU Hamburg–Harburg and his former coworker Dipl.-Phys. M. Krömer for supplying the single-phase version of the numerical code. The authors gratefully acknowledge the support from the Deutsche Forschungsgemeinschaft (DFG) within the scope of the Graduiertenkolleg ''Energie- und Umwelttechnik''.

Appendix A. Governing equations

For the simulation of 2-D inviscid cavitating flow, the following system of equations is solved under the assumption of constant temperature (see Section 2.4).

- fluid properties

$$\frac{\mathrm{d}x}{\mathrm{d}t} = (1-x)\cdot K_{\mathrm{l}\to\mathrm{v}}(T,p) - x\cdot K_{\mathrm{v}\to\mathrm{l}}(T,p) \tag{A.1}$$

- conservation of mass

$$\nabla\cdot\vec{c} = \rho\cdot\left(\frac{1}{\rho_{\mathrm{l}}}-\frac{1}{\rho_{\mathrm{v}}}\right)\cdot\frac{\mathrm{d}x}{\mathrm{d}t} \tag{A.2}$$

- conservation of momentum

$$\frac{\partial\rho\vec{c}}{\partial t} + \nabla\cdot\left(\rho\vec{c}\vec{c}\right) = -\nabla p \tag{A.3}$$

- transport of vapor fraction

$$\frac{\partial\alpha}{\partial t} + \nabla\cdot(\alpha\vec{c}) = -\frac{\rho}{\rho_{\mathrm{v}}}\frac{\mathrm{d}x}{\mathrm{d}t} \tag{A.4}$$

See Eqs. (6) and (7) for the relation of ρ, x and α.

References

Achenbach, M., Müller, I., 1985. Simulation of material behaviour of alloys with shape memory. Arch. Mech. 37 (6), 573–585.

Badur, J., Banaszkiewicz, M., 1998. A model of two-phase flow with relaxational-gradient microstructure. Proc. Third Int. Conf. on Multiphase Flow (ICMF '98), Lyon, France, CD-ROM.

Chen, R., Kirsh, Y., 1981. Analysis of Thermally Stimulated Processes. Pergamon Press, Oxford.

Delannoy, Y., Kueny, J.L., 1990. Two-phase flow approach in unsteady cavitation modelling. Cavitation and Multiphase Flow Forum, FED ASME 98, 153–158.

Dieval, L., Arnaud, M., Marcer, R., LeGouez, J.M., 1998. Improvement of a VOF method for multiphase flows. Proc. Third Int. Conf. on Multiphase Flow (ICMF '98), Lyon, France, CD-ROM.

Dreiß, A., 1997. Untersuchung der Laufradkavitation einer radialen Kreiselpumpe durch instationäre Druckmessungen im rotierenden System. Ph.D. thesis, Technische Universität Braunschweig, Verlag und Bildarchiv W.H. Faragallah.

Ferziger, J.H., Perić, M., 1996. Computational Methods for Fluid Dynamics. Springer-Verlag, Berlin.

Hairer, E., Wanner, G., 1991. Solving ordinary differential equations II. Stiff and differential-algebraic problems. Springer Series in Computational Mathematics. Springer-Verlag.

Isay, W.H., 1984. Kavitation. Schiffahrts-Verlag ''Hansa'' C. Schroedter & Co., second edition, Hamburg.

Lush, P.A., Peters, P.I., 1982. Visualization of the cavitating flow in a Venturi-type duct using high-speed cine photography. IAHR, Amsterdam.

Müller, I., 1994. Grundzüge der Thermodynamik. Springer-Verlag, Berlin.

Müller, I., Seelecke, S., 1993. Spezielle Probleme der Thermodynamik, Exercises on the Respective Lecture, Fachgebiet Thermodynamik, Technische Universität Berlin, Germany.

Numerical Algorithm Group (NAG). 2001. Routine Descriptions on Internet Pages: http://www.nag.co.uk/numeric/flolch/mk17/d/d01amf.html, http://www.nag.co.uk/numeric/flolch/mk17/d/d01ajf.html.

Pruß, A., Wagner, W., 2002. The IAPWS formulation1995 for the thermodynamic properties of ordinary water substance for general and scientific use. J. Phys. Chem. Ref. Data 31 (2), 387–536.

Stutz, B., Reboud, J.L., 1997. Experiments on unsteady cavitation. Exp. Fluids 22, 191–198.

Sauer, J., 2000. Instationär kavitierende Strömungen—Ein neues Modell basierend auf Front Capturing (VoF) und Blasendynamik. Ph.D. thesis, Fakultät für Maschinenbau, Universität Karlsruhe (TH), Germany, http://www.ubka.uni-karlsruhe.de/cgi-bin/psview?document=2000/maschinenbau/7.

Seelecke, S., 1999. Adaptive Strukturen mit Formgedächtnisaktoren—Modellierung und Simulation. Habilitation thesis, Technische Universität, Berlin, Germany.

Seelecke, S., Müller, I., 2003. Shape memory alloy actuators in smart structures modelling and simulation. Appl. Mech. Rev., to appear.

Vortmann, C., 2001. Untersuchungen zur Thermodynamik des Phasenübergangs bei der numerischen Berechnung kavitierender Düsenströmungen. Ph.D. thesis, Fakultät für Maschinenbau, Universität Karlsruhe (TH), Germany, http://www.ubka.uni-karlsruhe.de/cgi-bin/psview?document=2001/maschinenbau/4.